Applied Physics Letters

RESEARCH ARTICLE | JUNE 13 2023

Ising superconductivity: A first-principles perspective

Darshana Wickramaratne ; I. I. Mazin

Appl. Phys. Lett. 122, 240503 (2023)
https://doi.org/10.1063/5.0153345

Applied Physics Letters PERSPECTIVE pubs.aip.org/aip/apl

Ising superconductivity: A first-principles perspective

Cite as: Appl. Phys. Lett. **122**, 240503 (2023); doi: 10.1063/5.0153345
Submitted: 6 April 2023 · Accepted: 26 May 2023 ·
Published Online: 13 June 2023

Darshana Wickramaratne[1,a] and I. I. Mazin[2,3]

AFFILIATIONS

[1]Center for Computational Materials Science, U.S. Naval Research Laboratory, Washington, District of Colombia 20375, USA
[2]Department of Physics and Astronomy, George Mason University, Fairfax, Virginia 22030, USA
[3]Quantum Science and Engineering Center, George Mason University, Fairfax, Virginia 22030, USA

[a)]**Author to whom correspondence should be addressed:** darshana.wickramaratne@nrl.navy.mil

ABSTRACT

The recent discovery of Ising superconductivity has garnered much interest due in part to the resilience of these superconductors to large in-plane magnetic fields. In this Perspective, we explain the basic concepts that define the behavior of Ising superconductors, provide an overview of the electronic structure and magnetic properties with a focus on $NbSe_2$, summarize key experimental observations that have been made in this class of superconductors, highlight the role that defects and proximity-induced effects at interfaces have on Ising superconductivity, and finally discuss the prospects for observing Ising superconductivity in bulk materials.

Published by AIP Publishing. https://doi.org/10.1063/5.0153345

I. INTRODUCTION

A fundamental concept in the theory of superconductors is the paramagnetic limiting magnetic field (Clogston–Chandrasekar–Pauli-limiting field),[1,2] henceforth, referred to as the Pauli-limiting field. This is the approximate magnetic field where superconductivity is suppressed when the Zeeman splitting of the spin degenerate states at the Fermi level exceeds the magnitude of the superconducting gap. Recently, superconductivity in a number of two-dimensional materials was shown to be surprisingly resilient to an in-plane magnetic field that greatly exceeded the Pauli-limiting field. The first report of this large in-plane critical field was in gated single monolayer MoS_2, a two-dimensional transition metal dichalcogenide (TMD).[3] Shortly thereafter, large in-plane critical fields that exceeded the Pauli limit were found in a number of other two-dimensional materials, including monolayer $NbSe_2$,[4,5] TaS_2,[5] and gated WS_2.[6] Superconductors with thermodynamic critical fields, H_{c2}, that exceed the Pauli-limiting field are often associated with spin-triplet superconductors (since the Cooper pairs with parallel spins having the ability to screen the applied magnetic field), or due to the absence of a mirror plane in the material, which leads to an in-plane Rashba spin texture[7] or short spin–orbit scattering times in the plane of anisotropic layered materials,[8] both of which lead to large out-of-plane critical fields. The large in-plane critical magnetic fields in these two-dimensional materials, now referred to as Ising superconductors, have a very different intrinsic origin.

The large in-plane H_{c2} in the initial experiments on the monolayer TMDs was hypothesized to originate from the large spin–orbit splitting due to the transition metal in these TMDs. This was based on a general understanding that the Fermi surface of these hexagonal materials is comprised of two concentric Fermi rings around the K and K′ points of the Brillouin zone. The large spin–orbit coupling (SOC) of the transition metal splits the two Fermi contours within a given K valley, and the pseudospin direction is pinned along $\hat{z}$. This description of the Fermi surface has formed the basis for a number of model theories that have been put forth to analyze the experiments that have been reported on Ising superconductors.[9–12] We note that several authors have also provided an overview on the different materials where evidence for Ising superconductivity has been uncovered.[13–15] While these model theories have been used to both attempt to explain the wide range of experiments and also predict new phenomena, they are unable to establish material-specific insight into different phenomena.

In this Perspective, we offer a personal viewpoint on how first-principles calculations can be and have been used to elucidate the properties of Ising superconductors. Our aim is not to provide a comprehensive overview of the field of Ising superconductivity given that this remains an active area of research. Rather, our goal is to show how first-principles calculations enable insight into material-specific issues that are otherwise unattainable with model Hamiltonian descriptions of the electronic structure of the TMD monolayers.

While Ising superconductivity has been reported in a range of materials, our discussion will primarily focus on the example of the monolayer $NbSe_2$, the most widely studied Ising superconductor.

Our discussion will highlight the hierarchy of energy scales that provides a natural explanation for the large H_{c2} in these materials; the presence of magnetic fluctuations,[16,17] which we show are present in the TMDs that exhibit Ising superconductivity; and a detailed description of the fermiology, including the role of the third pocket at the zone-center. No material is ideal, including the TMD Ising superconductors. We will show that non-magnetic and magnetic point defects, which are likely to be present in these materials, can manifest themselves in interesting phenomena, such as apparent disorder-induced enhancement in superconductivity,[18,19] hysteresis in the superconducting phase,[20] oscillations in the superconducting current, and apparent breaking of rotational symmetry.[21,22]

This article is organized as follows: In Sec. II, we provide a general discussion of the physics of Ising superconductors; in Sec. III, we provide an overview of the electronic and magnetic properties of monolayer $NbSe_2$; in Sec. IV, we discuss the impact that defects, doping, and alloying have on the superconducting properties of Ising superconductors; in Sec. V, we show how experiments involving heterostructures with Ising superconductors lead to a number of puzzling results; and in Sec. VI, we show how Ising superconductivity phenomenon often associated with single monolayers can be found in bulk materials.

II. GENERAL CONSIDERATIONS

We first discuss at a general level the physics that leads to Ising superconductivity. We start from the simplest description of the Fermi surface of monolayer TMDs where Ising superconductivity is observed—two quasi-circular Fermi contours around the K and K′ valleys, which are related by time-reversal symmetry.

With spin–orbit interaction, the spin-degenerate states within a given valley are split by a spin–orbit coupling (SOC) parameter, Δ_{SOC}, resulting in two concentric Fermi contours as illustrated in Fig. 1(a). The pseudospin along $\hat{z}$ flips direction between the two Fermi contours such that within a given valley, there is a finite polarization of pseudospins as denoted by the colored area in Fig. 1(b). Moving from one valley (K) to its time-reversal partner (K′), the direction of the pseudospin flips as illustrated by the different colored areas in Fig. 1(b) so that the overall net magnetic moment is zero.

If we apply a magnetic field, H, parallel to the c-axis of the monolayer TMD, the Fermi contours within a given valley are Zeeman split by an amount that is linearly proportional to the magnitude of the magnetic field. Assuming that the magnetic field is applied along $+\hat{z}$, the Fermi contours derived from pseudospin $+\hat{z}$ will increase in area while those derived from $-\hat{z}$ will decrease. Hence, based on our notation in Fig. 1(a), the area between the two concentric Fermi contours will now be different between K and K′ as illustrated in Fig. 1(c). This manifests itself in a finite net spin polarization as expected by an amount that is proportional to the magnetic field and the single-spin density of states of the material (neglecting the Stoner enhancement).

When the magnetic field is perpendicular to the c-axis, the spins that are $\lesssim\Delta_{SOC}$ away from the Fermi level tilt away from $\hat{z}$. Since Δ_{SOC} is significantly larger than the magnitude of the Zeeman splitting and is also larger than the superconducting gap, Δ, the tilting of the spins away from $\hat{z}$ means that the spin susceptibility is defined by

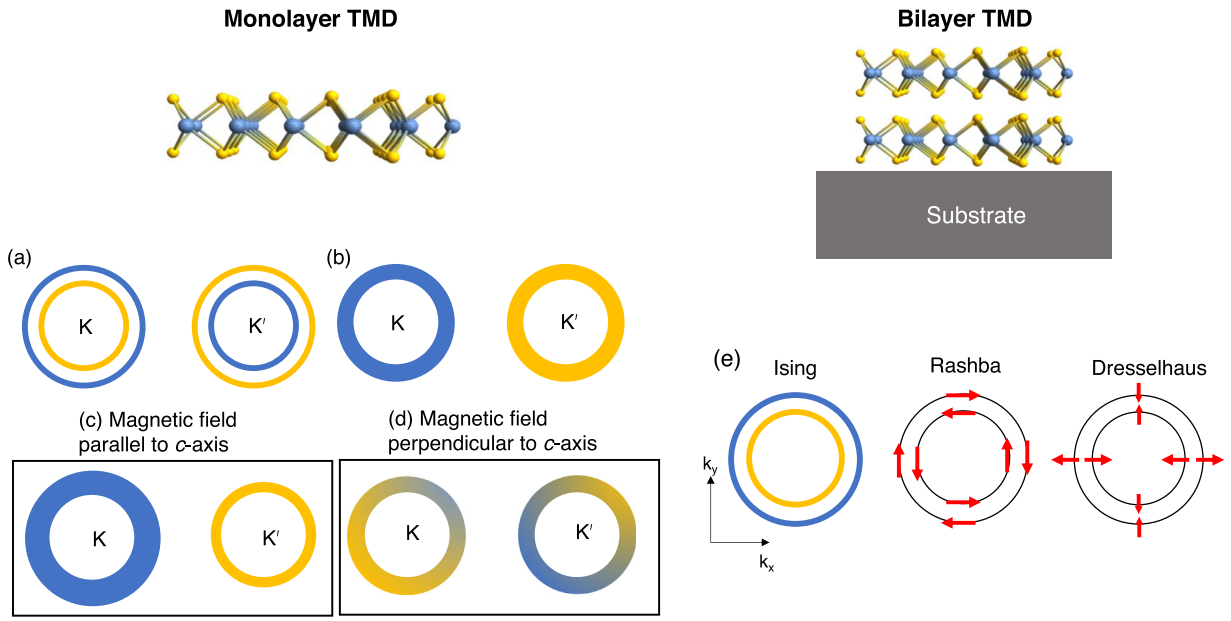

FIG. 1. (a) Schematic illustration of the Fermi contours around K and K′ in a monolayer TMD Ising superconductor in the presence of spin–orbit interaction. Blue represents $\hat{z}$ pseudospin states, and yellow represents $-\hat{z}$ pseudospin states. (b) Net pseudospin enclosed around each Fermi contour denoted by the area enclosed by the blue and yellow shaded regions. (c) Fermi contours and net pseudospin in the presence of a magnetic field that is parallel to the c-axis of the monolayer, i.e., parallel to the direction of the spins. (d) Fermi contours and the net pseudospin in the presence of an in-plane magnetic field, i.e., field is perpendicular to the direction of the spins. Note that the area bounded by the two Fermi contours within a given valley is similar in (b) and (d) but different in (c) due to the Zeeman splitting. (e) Possible in-plane spin textures (Rashba or Dresselhaus) in addition to the Ising spin texture in monolayer or few-layer TMDs due to symmetry lowering effects, e.g., substrate-induced effects as illustrated in the top right.

states that are approximately an energy Δ_{SOC} away from the Fermi level. To the first order in the magnitude of the in-plane magnetic field, there is no Zeeman splitting of the Fermi contours. As a result, the area between the two Fermi contours within a single valley does not change. However, there is a net spin polarization due to the fact that the pseudospins are tilted away from $\hat{z}$ to be in-plane in the two valleys.

With this heuristic understanding of the response of the electronic structure to out-of-plane and in-plane magnetic fields, it is now easy to address why Ising superconductors exhibit such a large anisotropy in their H_{c2}. The H_{c2} of a superconductor is determined by the difference in the free energies of the normal state and the superconducting state of a material. Within BCS theory and at 0 K, the thermodynamic critical field, H_{c0}, is defined as $F_n - F_s \sim \Delta^2 N(0)/2 = (\chi_n - \chi_s)H_0^2/2$, where $N(0)$ is the density of states at the Fermi level. Since the spin susceptibility for magnetic fields parallel to the c-axis is determined by the Zeeman splitting of the Fermi contours, superconductivity is suppressed once the magnitude of the Zeeman splitting exceeds Δ, i.e., the superconductivity is Pauli limited. In contrast, when the magnetic field is perpendicular to the c-axis the spin susceptibility is determined by states approximately Δ_{SOC} from the Fermi level. Since Δ_{SOC} is significantly larger than the magnitude of the Zeeman splitting induced by the applied magnetic field, H, and Δ, the in-plane H_{c2} is formally infinite in an Ising superconductor.

From this discussion, it is apparent that the hierarchy of energy scales that dictates this large in-plane H_{c2} is $H \leq \Delta \ll \Delta_{SOC}$. The combination of time-reversal symmetry and broken inversion symmetry guarantees that the pseudospin has pure $\pm\hat{z}$ character around the K valleys.

Moving from a monolayer to a bilayer leads to four bands that cross the Fermi level, forming two pairs degenerate in energy and comprised of equal contributions from both monolayers. Within a single K valley, the sign of the pseudospin flips from $+\hat{z}$ to $-\hat{z}$ between the pair of degenerate states. The second pair of degenerate states is an energy Δ_{SOC} away. This layer degeneracy of the states within a K valley is due to the centrosymmetric stacking of the two monolayers. The vertical stacking between the two monolayers leads to a finite interlayer hopping, t, between the monolayers. We will show in Sec. III that this interlayer hopping is k-dependent.

Additional terms can arise that impact the energy and spin character of these states. Indeed, Shaffer *et al.*[10] have shown that the coupling between a single monolayer and a substrate can introduce an in-plane component to the spin texture (Rashba and/or Dresselhaus) as illustrated in Fig. 1(e) in addition to the Ising component along $\hat{z}$. These considerations also apply to the bilayer structures. One additional consideration is changes in stacking away from the ground state centrosymmetric stacking, which can lead to changes in the interlayer hopping as well as to a non-centrosymmetric bilayer structure. Since the ground state stacking of the bulk $NbSe_2$ unit cell is centrosymmetric, there is often an implicit assumption that Ising superconductivity cannot survive in bilayer or bulk structures. However, in Sec. VI, we highlight experimental studies where evidence of Ising superconductivity in bulk compounds has indeed been observed and point to work, indicating that there is a region of the parameter space that involves Δ_{SOC}, interlayer hopping, and the coupling to a substrate/superstrate that leads to Ising protection in bilayer structures.

These general considerations provide qualitative insight into two hallmarks of Ising superconductivity—the large in-plane H_{c2} that greatly exceeds the Pauli-limiting field and the reduction in H_{c2} for few-layer and bulk films. In Secs. III–VI, we will discuss material-specific aspects of the electronic properties that provide insight that cannot be attained using the considerations that we have detailed above.

III. ELECTRONIC STRUCTURE

For the discussion that follows, we will focus on monolayer $NbSe_2$, which is the most widely studied Ising superconductor. The building block for monolayer $NbSe_2$ is a Nb atom that is in a trigonal prismatic coordination with the Se atoms. The overall structure is non-centrosymmetric and belongs to space group $P\bar{6}m2$. The trigonal crystal field splits the $4d$ states of Nb^{4+} into the following groups: d_{z^2}, $[d_{x^2-y^2}, d_{xy}]$, and $[d_{xz}, d_{yz}]$, which in the absence of SOC leads to a spin degenerate band that crosses the Fermi level several times. This band structure, which has been reported in several studies, leads to three Fermi contours, one that encircles Γ due to contributions from the Nb d_{z^2} states and a pair of Fermi contours that encircle the K and K′ points of the Brillouin zone that are contributed by the Nb $[d_{x^2-y^2}, d_{xy}]$ states. The combination of SOC due to Nb and the lack of an inversion center leads to momentum-dependent spin–orbit splitting everywhere except along the Γ–M line. The electronic structure of monolayer $NbSe_2$ is summarized in Fig. 2. Note that there is also a minor admixture of the Se p-states, where at Γ the Se p_z states contribute while at K the Se $p_{x,y}$ states contribute as illustrated in Fig. 2(b).

To understand this momentum-dependent spin–orbit splitting that pins the pseudospins to be along $\hat{z}$, we consider the bands that cross the Fermi level, a state at a given momentum k can be defined as $|\phi\rangle = \eta|d_{x^2-y^2}\rangle + \beta|d_{xy}\rangle + \gamma|d_{z^2}\rangle$, where $\eta^2 + \beta^2 + \gamma^2 = 1$. Here, we ignore the minor contribution of the chalcogen p-states to the bands that cross the Fermi level. Note that d_{z^2} corresponds to $|l, m\rangle = |2, 0\rangle$, $d_{x^2-y^2}$ to $(|2, 2\rangle + |2, -2\rangle)\sqrt{2}$, and d_{xy} corresponds to $(|2, 2\rangle - |2, -2\rangle)/i\sqrt{2}$, where l is the angular momentum quantum number and m is the magnetic quantum number.

When we account for spin, the Hamiltonian at each k-point is a (2×2) matrix. Since the single monolayers have $z/-z$ mirror symmetry around the Nb atom, the Hamiltonian does not include contributions from the $|2, \pm 1\rangle$ orbitals. Hence, the nondiagonal matrix elements $L_\pm$ are zero. However, the diagonal element can be defined as $L_z = 2(\eta \mathrm{Im}\beta - \beta \mathrm{Im}\eta)$. One phase can always be selected as real, for instance, η, which leads to $L_z = 2\eta \mathrm{Im}\beta$. Only along Γ–M is the value of β real by symmetry, which leads to $L_z = 0$ and zero splitting due to SOC. Elsewhere along the Brillouin zone, this leads to an orbital moment that can only be parallel or antiparallel with respect to $\hat{z}$. With the inclusion of spin–orbit coupling, this leads to the pseudospin to point along $\hat{z}$, which is indeed what we find in electronic structure calculations of monolayer $NbSe_2$. The spin–orbit induced splitting, which is maximal at K (and K′), depends largely on the transition metal element of the TMD monolayer. From density functional theory (DFT) calculations, the splitting at K is 150 meV in monolayer $NbSe_2$; in monolayer NbS_2, it is 115 meV, while it is 280 meV in monolayer TaS_2.

One of the experimental challenges when studying single monolayer films is that conventional bulk probes of the electronic structure of materials are not readily applied to single monolayer films. However, one can still obtain valuable information on the properties of the single monolayer by comparing the calculated and experimentally measured properties of the bulk compounds in addition to

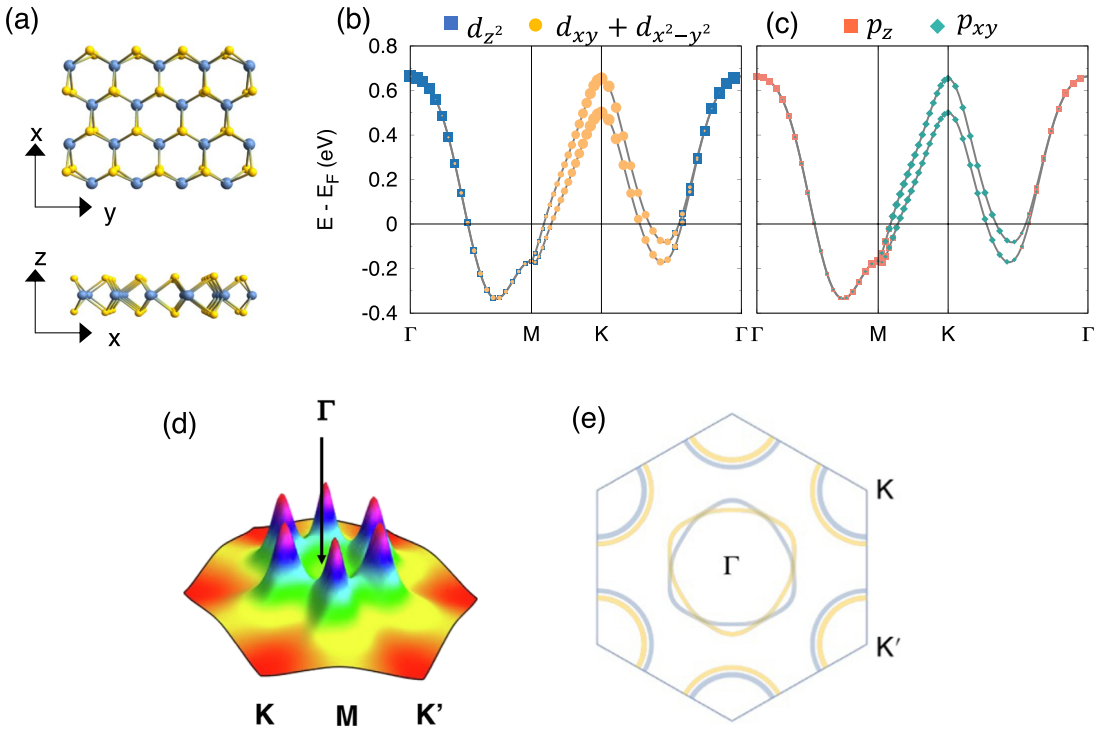

FIG. 2. Electronic properties of monolayer $NbSe_2$. (a) Top view and side view of monolayer $NbSe_2$ where Nb atoms (blue) are in a trigonal prismatic coordination with the Se atoms (yellow). (b-c) Band structure with SOC calculated with DFT of monolayer $NbSe_2$. The colors correspond to the contribution by the different *d* and *p* orbitals denoted in the legend above. (d) Renormalized spin susceptibility as a function of spin spiral **q** vector across the Brillouin zone of monolayer $NbSe_2$. (e) The Fermi contour of $NbSe_2$ where the colors denote the different pseudospin character of the states. Panel (d) was reproduced with permission from Das and Mazin, Comput. Mater. Sci. **200**, 110758 (2021). Copyright 2021 Elsevier.

comparisons of trends associated with calculated properties of the single monolayer vs bulk. Hence, it is instructive to briefly discuss the properties of bulk $NbSe_2$—a well-known superconductor although not an Ising superconductor.

The bulk $NbSe_2$ unit cell is comprised of two monolayers of $NbSe_2$ that are vertically stacked leading to a centrosymmetric structure that belongs to space group $P6_3/mmc$. Superconductivity, which has been measured below 7.2 K in bulk $NbSe_2$,[24,25] is widely thought to be driven entirely by the electron–phonon coupling.[26,27] First-principles calculations of the Fermi surface of bulk $NbSe_2$ at the level of the generalized gradient approximation are generally in agreement with ARPES measurements.[28,29]

One experimental fact that had largely been overlooked is spin susceptibility measurements of bulk $NbSe_2$, which reports a low temperature spin susceptibility of 3.04×10^{-4} emu/mole.[30] The Pauli susceptibility of bulk $NbSe_2$ using the DOS at the Fermi level from DFT calculations yields a spin susceptibility that is a factor of 3 lower than experiment. This is an indication of a considerable Stoner renormalization, corresponding to a Stoner factor $I \approx \frac{2}{3}N(0)$. On the other hand, the calculated Stoner-renormalized susceptibility is about 40% *larger* than the experimental number.[16]

This overestimation of the calculated spin susceptibility in comparison with experiment is a well-known consequence of using a mean field theory, such as the generalized gradient approximation implementation of DFT to calculate the properties of itinerant metals that are close a magnetic instability. Other examples of this overestimation in the calculated spin response at the DFT level in comparison with experiment include studies on bulk Pd[31] and the iron-based superconductors.[32] The magnetic moments and the tendency toward long-range magnetic order, which are overestimated at this mean field level in itinerant metals, are in reality suppressed due to the presence of long-range magnetic fluctuations.[33]

This difference in the calculated Pauli susceptibility and the experimental susceptibility of bulk $NbSe_2$, therefore, points to the presence of strong spin fluctuations in $NbSe_2$, which would renormalize the Pauli paramagnetic susceptibility. Further indirect evidence for the presence of spin fluctuations in the bulk structure is that state-of-the-art first-principles calculations of the superconducting T_c that only account for the electron–phonon coupling largely overestimate T_c compared to the experimentally established value.[34] This discrepancy is likely due to pair-breaking effects, such as spin fluctuations not being accounted for in the calculations.

Returning to the monolayer structure, the ferromagnetic spin susceptibility of monolayer $NbSe_2$ has been calculated to be a factor of 1.5 larger than the bulk, suggesting that spin fluctuations are, not unexpectedly, stronger in the single monolayer compared to bulk $NbSe_2$.[16] Das *et al.*[23] have also convincingly shown that monolayer $NbSe_2$ exhibits antiferromagnetic spin fluctuations with a **q** vector of

[0.2,0,0] as illustrated in Fig. 2(d). The role of magnetism in $NbSe_2$ has also been highlighted by a number of theoretical studies by other groups.[17,35]

There are several ramifications of this combination of the electronic structure and the presence of spin fluctuations on the Ising superconductivity. Arguably the most interesting ramifications of the presence of these spin fluctuations are on the pairing interactions. If we only consider Cooper pairs formed from states that reside at K and K′ (i.e., neglecting contributions at Γ), in the simplest approximation, one may assume that the amplitude of the order parameter across the two Fermi contours illustrated in Fig. 3 is similar. Since the pseudospins flip sign between K and K′, the formation of Cooper pairs due to phonons can only involve processes that do not require a change in the sign of the pseudospin. Superconducting states are either classified as singlet to triplet depending on whether the total spin of the Cooper pair is 0 or 1. One interesting consequence of the broken Kramer's degeneracy at the K and K′ valleys in the single monolayer TMDs is that the superconducting state is neither singlet nor triplet but a combination of singlet and triplet.[16]

To put these qualitative arguments on more firm, theoretical footing recent first-principles calculations[34] have determined the impact of the electron–phonon interaction and spin fluctuations on the pairing interactions in monolayer $NbSe_2$. The principal findings of this study are that (1) the electron–phonon interaction is highly anisotropic and the dominant pairing mechanism is due to intervalley processes between the Fermi contours with similar pseudospins at the K and K′ valleys (dotted black arrows in Fig. 3), (2) the T_c calculated due to electron–phonon interactions alone is greatly overestimated compared to the experimental T_c, and (3) spin fluctuations weaken the strength of pairing interactions and bring the calculated T_c in closer agreement with experiment. The fact that the calculated ferromagnetic spin susceptibility of the monolayer structure is larger than bulk $NbSe_2$ may also explain why the T_c of the bulk structure is larger than that of the monolayer.

Other competing mechanisms have also been proposed to be at play and impact superconductivity. The role of the charge density wave (CDW) phase in $NbSe_2$ and its impact on superconductivity continue to be actively debated. Some theoretical studies have proposed that the CDW phase is responsible for the reduction in the superconducting T_c compared to the T_c obtained entirely due to the electron–phonon interaction.[36] Irradiation experiments conducted on bulk $NbSe_2$ have suggested that there is a complex interplay between the CDW phase and the superconducting phase.[37] However, recent experiments have shown that the suppression of the CDW in monolayer $NbSe_2$ due to alloying with Mo also leads to a suppression of the superconducting T_c,[38] which is incompatible with the proposal in Ref. 36. Furthermore, applying pressure[39] has been shown to suppress the CDW while leading to a minor change in the superconducting transition temperature.

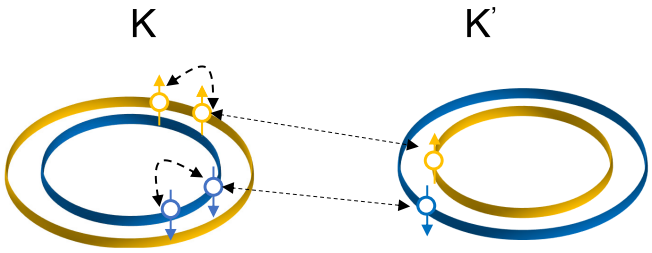

FIG. 3. Schematic illustration of Fermi contours around K and K′ illustrating the possible pairing interactions involving phonons. The yellow and blue contours represent states with pseudospin $m_z = 1+$ or $m_z = 1-$, respectively. The black dashed and dotted arrows denote intravalley and intervalley pairing interactions that can occur due to the electron–phonon interaction.

Recent tunneling measurements on monolayer $NbSe_2$, which observed a number of satellite peaks on either side of the primary coherence peaks, were interpreted as a manifestation of a Leggett mode between a singlet *s*-wave and a spin-triplet *f*-wave channel.[38] We note, however, that this postulation is incompatible with the findings of first-principles calculations[34] where it was shown that the *f*-wave pairing interactions within the K valley are weak. Other tunneling measurements in the presence of an in-plane magnetic field have interpreted their measurements by pointing to the possible presence of a subleading spin-triplet order parameter.[40] Transport measurements in the presence of an in-plane magnetic field found a surprising twofold periodicity in the magnetoresistance, which was interpreted as evidence of a competing nematic superconducting instability[22] that coexists with a conventional singlet superconducting state. In order to confirm the experimental manifestation of these proposed mechanisms, another issue to contend with is the role of defects and disorder, which we discuss in Sec. IV.

IV. DEFECTS, DOPING AND ALLOYING

Experiments on the role of disorder either through alloying, doping, or defects have led to a number of puzzling results. Alloying $NbSe_2$ with sulfur (which is isovalent to selenium) was found to change T_c non-monotonically with sulfur content—a pronounced increase in T_c up to a critical sulfur content subsequently followed by a monotonic suppression. Qualitatively similar non-monotonic changes in T_c were found in $NbSe_2$ that had been exposed to silicon.[18] This increase in T_c for intermediate concentrations of the alloying element was postulated to be evidence of fractal superconductivity—i.e., a disorder-induced enhancement of superconductivity. However, this purported enhancement was reported with respect to $NbSe_2$ samples that had a T_c of ∼1 K—significantly lower than the widely reported value of 3–4 K. Finally, doping $NbSe_2$ with Mo was found to enhance T_c slightly up to a critical concentration of doping after which superconductivity was suppressed.[41] These changes in T_c with doping in monolayer $NbSe_2$ are summarized in Fig. 4(a).

Interpreting the experiments on alloying or doping requires information on where in the lattice, the impurity is incorporated since this determines the electrical properties of the impurity. For example, when Mo is incorporated in $NbSe_2$, it incorporates substitutionally on the Nb site as shown by STM studies[41] and further corroborated by first-principles calculations [cf. Fig. 4(b)]. The extra electron from Mo dopes $NbSe_2$. This leads to a narrow range of doping where T_c is initially enhanced beyond which T_c gradually decreases and superconductivity is suppressed at a critical Mo composition. Doping $NbSe_2$ with Mo leads to a monotonic reduction in the density of states, which leads to two effects. It decreases the magnitude of the electron–phonon coupling that is responsible for pairing, which suppresses T_c, and it would also suppress the magnitude of pair-breaking magnetic fluctuations, which would enhance T_c as illustrated in Fig. 4(c). It is likely that a combination of these two changes as a function of doping leads to

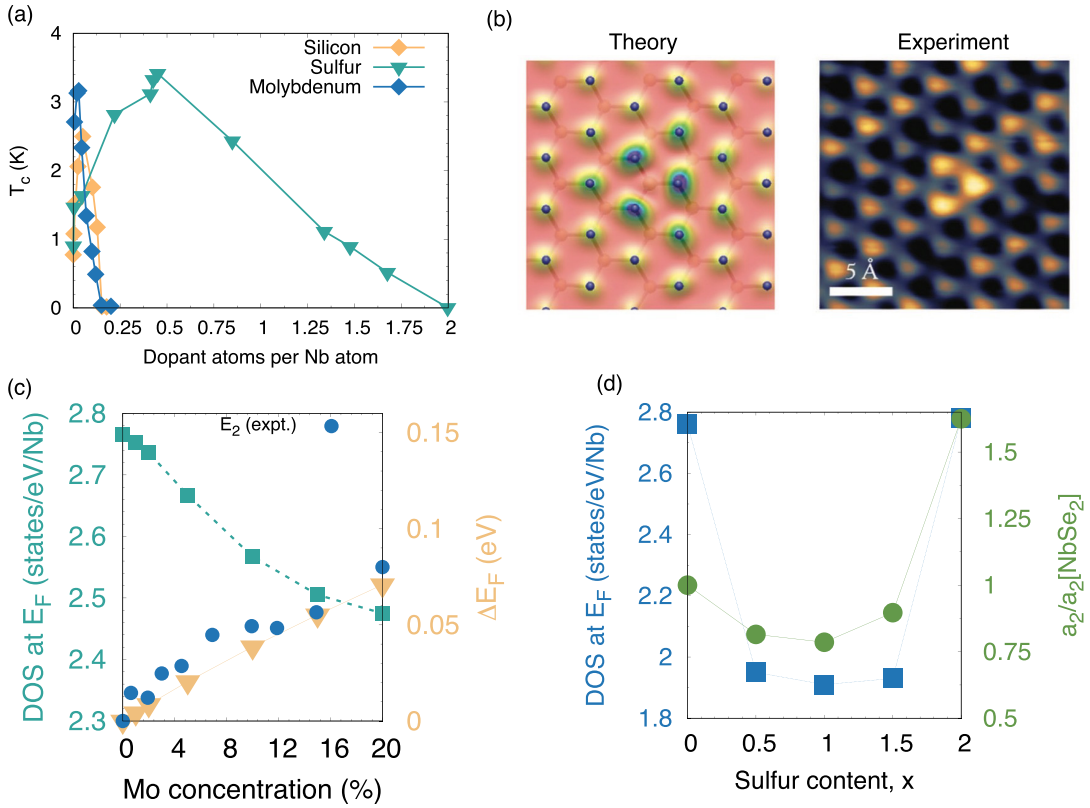

FIG. 4. Effect of alloying and doping in monolayer $NbSe_2$. (a) Summary of experimental reports on change in T_c as a function of alloying monolayer $NbSe_2$ with sulfur, silicon, and molybdenum. (b) Comparison of STM images from experiment and DFT calculations for substitutional Mo in $NbSe_2$. (c) First-principles calculations of the effect of alloying Mo in $NbSe_2$ on the density of states at the Fermi level and the shift in the Fermi level as a function of Mo content. Data points from experiment are included as blue dots. (d) First-principles calculations of the effect of alloying on the Se site with S on the density of states (left vertical axis) and the magnitude of ferromagnetic spin fluctuations normalized with respect to monolayer $NbSe_2$ (right vertical axis). Panels (b) and (c) were reproduced from Wan *et al.* Adv. Mater. **34**, 2200492 (2022). Copyright 2022 Wiley. Panel (d) was reproduced with permission from Wickramaratne and Mazin, Nat. Commun. 13, 2376 (2022). Copyright 2021 Author(s), licensed under a Creative Commons License.

the non-monotonic change in T_c that has been observed in experiments where $NbSe_2$ is doped with Mo.

A number of experiments have also explored the impact of alloying $NbSe_2$ with isovalent elements across the entire composition range showing a surprising enhancement in T_c as illustrated in Fig. 4(a). At this point, it is useful to recall that based on Anderson's theorem, non-magnetic impurities will not lead to pair-breaking in a conventional *s*-wave superconductor. However, magnetic impurities are pair-breaking. The tendency toward magnetism in these materials suggests that native point defects may lead to finite magnetic moments. Indeed, first-principles calculations have shown selenium vacancies to have low formation energies.[42] These calculations have also uncovered a large modulation of the spin density that extends several lattice sites away from the vacancy with a magnetic moment amplitude of $\sim 0.5\,\mu_B$.[43] If selenium vacancies are magnetic point defects in $NbSe_2$, this would provide a natural explanation for a number of experimental puzzles observed when monolayer $NbSe_2$ has been alloyed with sulfur and silicon.

First, selenium vacancies can act as a source of scattering and lower the residual resistivity ratio. The magnetic nature of these vacancies would also render them pair-breaking leading to a lower T_c. This also coincides with the fact that in the experiments, low values of the residual resistivity ratio were found in samples where the T_c of monolayer $NbSe_2$ was low.[37] Furthermore, in the experiments where sulfur and silicon were alloyed into $NbSe_2$, it was assumed that the $NbSe_2$ monolayer prior to alloying was stoichiometric and in the case of silicon that Si was being adsorbed on the surface.[18] Our first-principles calculations have shown that this assumption is incorrect, and depending on the concentration of selenium vacancies that are incorporated during growth, sulfur and silicon can occupy these vacant selenium sites.[42] This can lead to non-monotonic changes in the electronic and magnetic properties of $NbSe_2$ as a function of alloy content as shown in Fig. 4(d), and it is likely these non-monotonic changes in the electronic and magnetic properties that lead to non-monotonic change in T_c, not fractal superconductivity.

Non-magnetic defects in the presence of a magnetic field can also have nontrivial effects in Ising superconductors. Let us first consider an Ising superconductor with non-magnetic impurities in the absence of a magnetic field. Intervalley scattering between the two outer (or inner) contours is not permitted since this requires a spin flip.

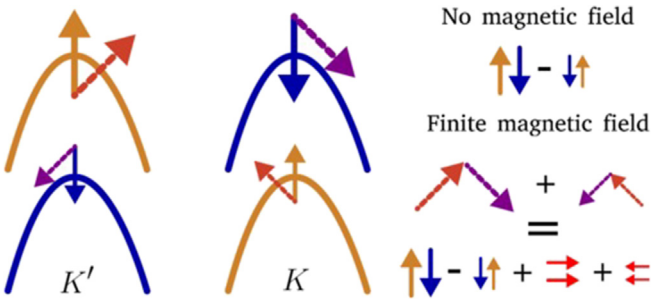

FIG. 5. Schematic illustration of the effect of a magnetic field on the canting of the spins at the K and K′ points. Reproduced with permission from Mockli and Khodas, Phys. Rev. B **101**, 014510 (2020). Copyright 2020 American Physical Society.

If H is parallel to $\hat{z}$, there is Zeeman splitting, which suppresses superconductivity but the conditions that prohibit intervalley scattering between the contours where a spin flip is required remain the same. Hence, no scattering occurs since the pseudospin remains pinned to $\hat{z}$. When H is in-plane, the spins around the K and K′ valleys tilt in-plane in the direction of H as discussed in Sec. II and illustrated in Fig. 5, acquiring a triplet component.

Since the pseudospins now have a finite in-plane component, intervalley scattering between the outer (and inner) contours due to non-magnetic impurities is allowed due to the finite overlap of spin states. Since the degree by which the pseudospins tilt away from $\hat{z}$ to be in-plane is proportional to the magnitude of the applied in-plane magnetic field, the magnitude of the scattering is expected to increase as a function of the magnitude of the magnetic field. This interplay between the Ising spin–orbit coupling, non-magnetic impurities, and scattering induced by an in-plane magnetic field would be expected to lead to a broadening of the coherence peaks associated with tunneling due to an Ising superconductor. Indeed, this prediction manifests itself in recent tunneling experiments that have been performed on $NbSe_2$ tunneling heterostructures where $CrBr_3$ was used as a magnetic insulator tunnel barrier, which we discuss in Sec. V.

V. HETEROSTRUCTURES WITH MAGNETIC AND NON-MAGNETIC INSULATORS

Since the Ising superconductors are two-dimensional materials, they also represent an ideal platform to explore the role of interfaces and the interaction of Ising superconductivity with different phenomenon, such as magnetism, charge density waves, and topological order. One such heterostructure is atomically thin Josephson junction heterostructures where the Ising superconductor is used as the top and bottom superconducting contacts sandwiched between an insulating barrier, such as WSe_2 or MoS_2[40,45] or magnetic insulating barriers, such as $CrBr_3$[22] to $Cr_2Ge_2Te_6$[20,46,47] as summarized in Fig. 6. In the case of the experiments that use WSe_2 as a tunnel barrier, the tunneling measurements that were performed in the presence of an in-plane magnetic field find evidence of equal spin-singlet-triplet pairs in the tunneling conductance.

In the case of the experiments with the magnetic insulating barriers, even though the barrier materials are different, there are a number of unifying observations. This includes the observation of an apparent enhancement of Δ along a surprising strengthening of the coherent peak width in tunneling, hysteresis that sets in below the superconducting T_c, evidence of broken rotational symmetry that occurs only in the superconducting state, and spin-filtering tunneling processes.[20,22,46,47] One idea put forth to explain the apparent symmetry breaking is the possibility of a two-component order parameter

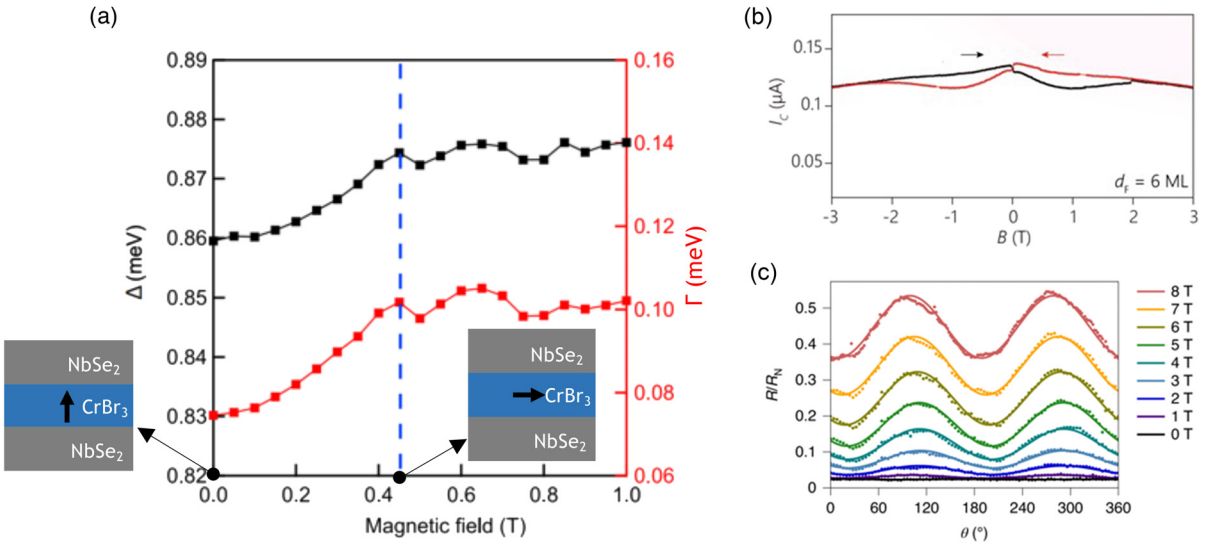

FIG. 6. Tunneling measurements in $NbSe_2$-magnetic insulator heterostructures. (a) Schematic illustration of the device geometry used in tunneling experiments along with measurements of the change in the superconducting gap and coherence peaks as a function of in-plane magnetic field reported in Ref. 48. Figure reproduced with permission from Kang *et al.*, arXiv:2101.01327 (2021). Copyright 2021 Author(s), licensed under a Creative Commons License. (b) Hysteresis in the switching current of the $NbSe_2$/$Cr_2Ge_2Te_6$/$NbSe_2$ junction as a function of applied in-plane magnetic field. Figure reproduced with permission from Idzuchi *et al.* Nat. Commun. 12, 5332 (2021). Copyright 2021 Author(s), licensed under a Creative Commons License. (c) Field dependence of the magnetoresistance in a $NbSe_2$/$CrBr_3$ heterostructure. Figure reproduced with permission from Hamill *et al.* Nat. Phys. **17**, 949 (2021). Copyright 2021 Springer Nature.

where a nematic phase coexists with the Ising superconducting phase in $NbSe_2$. It was postulated that the formation of such a heterostructure can couple to both order parameters, and the nematic phase would be responsible for the rotational symmetry breaking observed in the experiments.[21] Another possible explanation for this rotational symmetry breaking is the role played by non-magnetic defects, which in the presence of an in-plane magnetic field can behave as pair-breaking defects and lead to signatures that are consistent with those reported in experiment.[43,44]

An alternative approach to explore magnetic-Ising superconductor interfaces is to replace the magnetic layer that is in proximity with the Ising superconductor with magnetic transition metal ions that are intercalated. Such approaches have been explored experimentally in few-layer $NbSe_2$ and NbS_2 layers where magnetic ions, such as Cr and Fe, are intercalated in between the layers.[49–51] The intercalated ions have been shown to form an ordered superlattice within the basal plane of the TMD. These superlattices, such as $Fe_{1/3}NbS_2$, exhibit degenerate magnetic states[49] that are tunable by the concentration of magnetic ions that are intercalated. The impact of these intercalated ions and magnetic phases on superconductivity remains to be addressed. One intriguing possibility is the potential to observe signatures of Ising superconductivity in these intercalated structures given that Ising superconductivity can occur in bulk structures as we will discuss in Sec. VI.

VI. ISING SUPERCONDUCTIVITY IN BULK MATERIALS

The principal signature of Ising superconductivity is a large in-plane H_{c2}, which is pronounced in single monolayers of the superconducting TMDs. Surprisingly, experiments have shown that a range of bulk materials that are comprised of the TMDs exhibit large values of in-plane H_{c2}, which are comparable to those found in single monolayers. This includes experiments performed on misfit compounds that contain monolayers of NbS_2 and $NbSe_2$ sandwiched in between LaS and LaSe layers,[52–56] twisted monolayers of TaS_2,[57] bulk TaS_2 intercalated with different organic molecules,[58,59] and the 4H, 3R, and 6R polymorphs of $TaSe_2$ and TaS_2.[60–63] The early reports of these large in-plane H_{c2} values were interpreted as arising from spin–orbit scattering (using short spin–orbit scattering times) or the presence of a Rashba-like spin texture of the states at the Fermi surface, which would enable in principle finite-momentum pairing.[56] A majority of these proposed interpretations were made without taking into account the electronic structure of these misfit compounds and assessing whether the details of the Fermi surface would in fact favor Ising superconductivity.

We suggest that in each of these experiments, the large in-plane H_{c2} is likely a manifestation of Ising superconductivity in bulk compounds. The ground state stacking of the metallic TMDs is $2H_a$, which is centrosymmetric with a center of inversion between the layers. In some misfit compounds, the misfit layer is intercalated between the pair of TMD monolayers, thereby weakening the interlayer coupling of the bilayer structure. In other misfit compounds, such as $(LaSe)_{1.14}(NbSe_2)_2$, which is schematically illustrated in Fig. 7(a), the misfit layer is intercalated between pairs of the bilayer TMD that are stacked in their equilibrium $2H_a$ stacking. In both configurations, the misfit layer leads to doping of the TMD layers. First-principles calculations combined with photoemission data have recently shown that the states at the Fermi level in these misfit compounds are best described as a heavily electron-doped TMD layer.[55] Interestingly, these bulk misfit compounds exhibit in-plane H_{c2} values that greatly exceed the Pauli limit.[54]

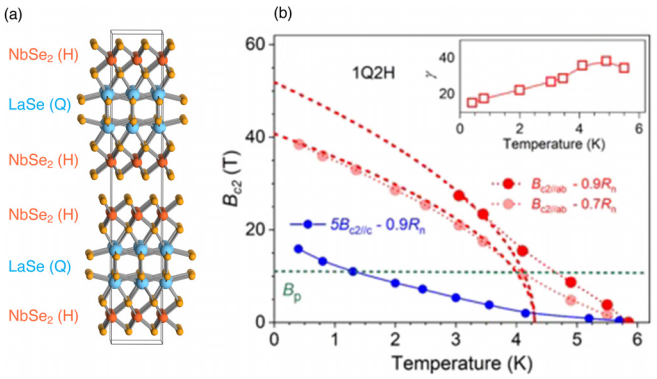

FIG. 7. Ising superconductivity in bulk compounds. (a) Schematic illustration of the $(LaSe)_{1.14}(NbSe_2)_2$ misfit compound where evidence of large in-plane critical fields that exceed the Pauli limit was measured. (b) Experimental reports of the in-plane critical field as a function of temperature for bulk misfit compounds that contain $NbSe_2$ layers. Reproduced with permission from Samuely *et al.*, Phys. Rev. B **104**, 224507 (2021). Copyright 2021 American Physical Society.

A natural question then is what leads to the large values of H_{c2} in these bulk compounds. In the case of the misfit compounds where the misfit layer is intercalated in between the bilayer TMD, the increase in the interlayer separation is sufficient to weaken the interlayer coupling so that the TMDs in the misfit act as two decoupled monolayers. Even though these monolayers are doped, the Fermi level shifts to an energy where the Ising protection is still present. In the misfit compounds where the misfit layer is in between a pair of bilayers, one aspect to consider is that the misfit layer above and below the bilayer is stacked asymmetrically. This can lead to an asymmetric on-site potential that effectively breaks the layer degeneracy that is otherwise present in the electronic structure of the bilayer. Identifying the competition between the relevant energy scales—Δ_{SOC}, interlayer coupling between the TMD layers with different stacking configurations of the misfit layer—and the combined effect of all of this on the details of the Fermi surface are parameters that can be extracted using first-principles calculations. Indeed, there is a range of parameter space where bilayer and bulk misfit compounds comprised of the TMDs can exhibit signatures of Ising superconductivity, such as large in-plane H_{c2}.[64] Given the wide range of misfit compounds where large values of in-plane H_{c2} have been observed,[52–56,65,66] we expect that these calculations when analyzed in the context of the experiments will play a key role in unraveling this signature of Ising superconductivity in these bulk compounds.

Another route to access Ising superconductivity in bulk materials is considering the fact that while the ground state stacking of the bulk TMDs is centrosymmetric, there are a large number of polytypes that these materials can exist in due to the different stacking configurations that are possible. We list some of these polytypes in Table I and schematically illustrate their stacking configurations in Fig. 8. We note that some of these polytypes, such as the 3R and 4Ha configuration, are not centrosymmetric, and indeed, there have been experimental reports of Ising superconductivity in these bulk polytypes.[66]

TABLE I. List of some of the possible polytypes of the bulk TMDs, their space group, whether they are centrosymmetric or not and if they belong to a symmorphic space group or not.

Polytype	Space group (#)	Centrosymmetric?	Symmorphic?
2H	$P6_3/mmc$ (190)	✓	×
3R	R3m (160)	×	✓
4Ha	P3m1 (156)	×	✓
4Hb	$P6_3/mmc$ (194)	✓	×

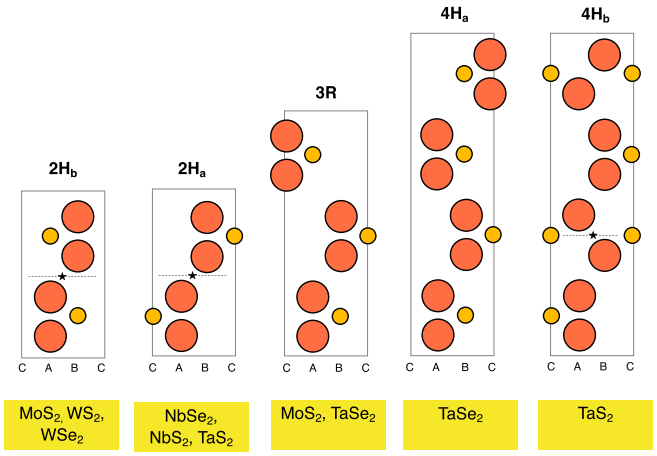

FIG. 8. Different polytypes of the bulk transition metal dichalcogenides. The transition metal is denoted with the small yellow circles and the chalcogens with the large red circles. The labels A, B, and C at the bottom can be used to determine the stacking sequence of each polytype. For the centrosymmetric stacking configurations, the center of inversion is denoted with a black star and a black dotted line. The materials where these polytypes have been identified are listed in a yellow box. Reproduced with permission from Brown and Beerntsen, Acta Crystallogr. 18, 31 (1965). Copyright 1965 Elsevier.[67]

VII. CONCLUSIONS

Since the first report of Ising superconductivity in two-dimensional materials in 2015, the number of materials that exhibit large in-plane magnetic fields, which is a signature of Ising superconductivity, has grown to include a wide range of low-dimensional materials. There is sometimes a myth (which we show to be unfounded) that Ising superconductivity is a rather esoteric phenomenon. In this Perspective article, we discuss how Ising superconductivity can in fact be understood at the basic level using our general understanding of the electronic structure of Ising superconductor materials and thermodynamic arguments for the susceptibility in the normal and superconducting state. Beyond providing this heuristic understanding, one of the major themes of this Perspective article is that first-principles calculations provide material-specific microscopic insight into the wide variety of experiments that have been performed thus far on Ising superconductors. We highlighted the important role played by non-magnetic and magnetic point defects and proximity-induced effects at interfaces in Ising superconductor heterostructures. Finally, we show that Ising superconductivity is not a phenomenon that only occurs in two-dimensional materials—there are a wide range of bulk misfit superconductors where Ising superconductivity is likely to occur as well.

ACKNOWLEDGMENTS

We thank Daniel Agterberg for helpful discussions. D.W. was supported by the Office of Naval Research through the Naval Research Laboratory's Basic Research Program. I.I.M. was supported by the Office of Naval Research through Grant No. N00014-20-1-2345.

AUTHOR DECLARATIONS

Conflict of Interest

The authors have no conflicts to disclose.

Author Contributions

Darshana Wickramaratne: Conceptualization (equal); Writing – original draft (lead); Writing – review & editing (equal). **Igor Mazin:** Conceptualization (equal); Writing – review & editing (equal).

DATA AVAILABILITY

Data sharing is not applicable to this article as no new data were created in this study.

REFERENCES

[1]A. M. Clogston, Phys. Rev. Lett. **9**, 266 (1962).
[2]B. Chandrasekhar, Appl. Phys. Lett. **1**, 7–8 (1962).
[3]J. Lu, O. Zheliuk, I. Leermakers, N. F. Yuan, U. Zeitler, K. T. Law, and J. Ye, Science **350**, 1353 (2015).
[4]X. Xi, Z. Wang, W. Zhao, J.-H. Park, K. T. Law, H. Berger, L. Forró, J. Shan, and K. F. Mak, Nat. Phys. **12**, 139 (2016).
[5]S. C. de la Barrera, M. R. Sinko, D. P. Gopalan, N. Sivadas, K. L. Seyler, K. Watanabe, T. Taniguchi, A. W. Tsen, X. Xu, D. Xiao, and B. Hunt, Nat. Commun. **9**, 1427 (2018).
[6]J. Lu, O. Zheliuk, Q. Chen, I. Leermakers, N. E. Hussey, U. Zeitler, and J. Ye, Proc. Natl. Acad. Sci. **115**, 3551 (2018).
[7]M. Smidman, M. B. Salamon, H. Q. Yuan, and D. F. Agterberg, Rep. Prog. Phys. **80**, 036501 (2017).
[8]R. A. Klemm, A. Luther, and M. Beasley, Phys. Rev. B **12**, 877 (1975).
[9]B. T. Zhou, N. F. Yuan, H.-L. Jiang, and K. T. Law, Phys. Rev. B **93**, 180501 (2016).
[10]D. Shaffer, J. Kang, F. Burnell, and R. M. Fernandes, Phys. Rev. B **101**, 224503 (2020).
[11]D. Möckli and M. Khodas, Phys. Rev. B **98**, 144518 (2018).
[12]E. Sosenko, J. Zhang, and V. Aji, Phys. Rev. B **95**, 144508 (2017).
[13]D. Zhang and J. Falson, Nanotechnology **32**, 502003 (2021).
[14]C. Wang, Y. Xu, and W. Duan, Acc. Mater. Res. **2**, 526 (2021).
[15]W. Li, J. Huang, X. Li, S. Zhao, J. Lu, Z. V. Han, and H. Wang, Mater. Today Phys. **21**, 100504 (2021).
[16]D. Wickramaratne, S. Khmelevskyi, D. F. Agterberg, and I. Mazin, Phys. Rev. X **10**, 041003 (2020).
[17]S. Divilov, W. Wan, P. Dreher, E. Bölen, D. Sánchez-Portal, M. M. Ugeda, and F. Ynduráin, J. Phys.: Condens. Matter **33**, 295804 (2021).
[18]K. Zhao, H. Lin, X. Xiao, W. Huang, W. Yao, M. Yan, Y. Xing, Q. Zhang, Z.-X. Li, S. Hoshino *et al.*, Nat. Phys. **15**, 904 (2019).
[19]C. Rubio-Verdu, A. M. Garcia-Garcia, H. Ryu, D.-J. Choi, J. Zaldivar, S. Tang, B. Fan, Z.-X. Shen, S.-K. Mo, J. I. Pascual, and M. M. Ugeda, Nano Lett. **20**, 5111 (2020).
[20]H. Idzuchi, F. Pientka, K.-F. Huang, K. Harada, Ö. Gül, Y. J. Shin, L. Nguyen, N. Jo, D. Shindo, R. Cava *et al.*, Nat. Commun. **12**, 5332 (2021).

[21]C.-W. Cho, J. Lyu, L. An, T. Han, K. T. Lo, C. Y. Ng, J. Hu, Y. Gao, G. Li, M. Huang *et al.*, Phys. Rev. Lett. **129**, 087002 (2022).
[22]A. Hamill, B. Heischmidt, E. Sohn, D. Shaffer, K.-T. Tsai, X. Zhang, X. Xi, A. Suslov, H. Berger, L. Forró *et al.*, Nat. Phys. **17**, 949 (2021).
[23]S. Das and I. I. Mazin, Comput. Mater. Sci. **200**, 110758 (2021).
[24]R. Frindt, Phys. Rev. Lett **28**, 299 (1972).
[25]J. Fletcher, A. Carrington, P. Diener, P. Rodiere, J.-P. Brison, R. Prozorov, T. Olheiser, and R. Giannetta, Phys. Rev. Lett. **98**, 057003 (2007).
[26]E. Boaknin, M. Tanatar, J. Paglione, D. Hawthorn, F. Ronning, R. Hill, M. Sutherland, L. Taillefer, J. Sonier, S. Hayden *et al.*, Phys. Rev. Lett. **90**, 117003 (2003).
[27]Y. Noat, J. Silva-Guillén, T. Cren, V. Cherkez, C. Brun, S. Pons, F. Debontridder, D. Roditchev, W. Sacks, L. Cario *et al.*, Phys. Rev. B **92**, 134510 (2015).
[28]M. Johannes, I. Mazin, and C. Howells, Phys. Rev. B **73**, 205102 (2006).
[29]K. Rossnagel, O. Seifarth, L. Kipp, M. Skibowski, D. Voß, P. Krüger, A. Mazur, and J. Pollmann, Phys. Rev. B **64**, 235119 (2001).
[30]M. Iavarone, R. Di Capua, G. Karapetrov, A. Koshelev, D. Rosenmann, H. Claus, C. Malliakas, M. G. Kanatzidis, T. Nishizaki, and N. Kobayashi, Phys. Rev. B **78**, 174518 (2008).
[31]P. Larson, I. Mazin, and D. Singh, Phys. Rev. B **69**, 064429 (2004).
[32]I. Mazin, M. Johannes, L. Boeri, K. Koepernik, and D. J. Singh, Phys. Rev. B **78**, 085104 (2008).
[33]T. Moriya, *Spin Fluctuations in Itinerant Electron Magnetism* (Springer Science & Business Media, 2012), Vol. 56.
[34]S. Das, H. Paudyal, E. Margine, D. Agterberg, and I. Mazin, npj Comput. Mater. **9**, 66 (2023).
[35]A. T. Costa, M. Costa, and J. Fernández-Rossier, Phys. Rev. B **105**, 224412 (2022).
[36]F. Zheng and J. Feng, Phys. Rev. B **99**, 161119 (2019).
[37]K. Cho, M. Kończykowski, S. Teknowijoyo, M. A. Tanatar, J. Guss, P. Gartin, J. M. Wilde, A. Kreyssig, R. McQueeney, A. I. Goldman *et al.*, Nat. Commun. **9**, 2796 (2018).
[38]W. Wan, P. Dreher, D. Muñoz-Segovia, R. Harsh, H. Guo, A. J. Martínez-Galera, F. Guinea, F. de Juan, and M. M. Ugeda, Adv. Mater. **34**, 2206078 (2022).
[39]M. Leroux, I. Errea, M. Le Tacon, S.-M. Souliou, G. Garbarino, L. Cario, A. Bosak, F. Mauri, M. Calandra, and P. Rodière, Phys. Rev. B **92**, 140303 (2015).
[40]M. Kuzmanović, T. Dvir, D. Leboeuf, S. Ilić, M. Haim, D. Möckli, S. Kramer, M. Khodas, M. Houzet, J. Meyer *et al.*, Phys. Rev. B **106**, 184514 (2022).
[41]W. Wan, D. Wickramaratne, P. Dreher, R. Harsh, I. I. Mazin, and M. M. Ugeda, Adv. Mater. **34**, 2200492 (2022).
[42]D. Wickramaratne and I. Mazin, Nat. Commun. **13**, 2376 (2022).
[43]D. Wickramaratne, M. Haim, M. Khodas, and I. I. Mazin, Phys. Rev. B **104**, L060501 (2021).
[44]D. Möckli and M. Khodas, Phys. Rev. B **101**, 014510 (2020).
[45]T. Dvir, F. Massee, L. Attias, M. Khodas, M. Aprili, C. H. Quay, and H. Steinberg, Nat. Commun. **9**, 598 (2018).
[46]K. Kang, H. Berger, K. Watanabe, T. Taniguchi, L. Forró, J. Shan, and K. F. Mak, Nano Lett. **22**, 5510 (2022).
[47]L. Ai, E. Zhang, J. Yang, X. Xie, Y. Yang, Z. Jia, Y. Zhang, S. Liu, Z. Li, P. Leng *et al.*, Nat. Commun. **12**, 6580 (2021).
[48]K. Kang, S. Jiang, H. Berger, K. Watanabe, T. Taniguchi, L. Forró, J. Shan, and K. F. Mak, arXiv:2101.01327 (2021).
[49]S. Wu, Z. Xu, S. C. Haley, S. F. Weber, A. Acharya, E. Maniv, Y. Qiu, A. Aczel, N. S. Settineri, J. B. Neaton *et al.*, Phys. Rev. X **12**, 021003 (2022).
[50]S. C. Haley, E. Maniv, T. Cookmeyer, S. Torres-Londono, M. Aravinth, J. Moore, and J. G. Analytis, arXiv:2111.09882 (2021).
[51]L. S. Xie, S. Husremovic, O. Gonzalez, I. M. Craig, and D. K. Bediako, J. Am. Chem. Soc. **144**, 9525 (2022).
[52]Y. Kashihara, A. Nishida, and H. Yoshioka, J. Phys. Soc. Jpn. **46**, 1112 (1979).
[53]R. Coleman, G. Eiserman, S. Hillenius, A. Mitchell, and J. Vicent, Phys. Rev. B **27**, 125 (1983).
[54]P. Samuely, P. Szabó, J. Kačmarčík, A. Meerschaut, L. Cario, A. Jansen, T. Cren, M. Kuzmiak, O. Šofranko, and T. Samuely, Phys. Rev. B **104**, 224507 (2021).
[55]R. T. Leriche, A. Palacio-Morales, M. Campetella, C. Tresca, S. Sasaki, C. Brun, F. Debontridder, P. David, I. Arfaoui, O. Šofranko *et al.*, Adv. Funct. Mater. **31**, 2007706 (2021).
[56]A. Devarakonda, T. Suzuki, S. Fang, J. Zhu, D. Graf, M. Kriener, L. Fu, E. Kaxiras, and J. Checkelsky, Nature **599**, 51 (2021).
[57]Y. Ma, J. Pan, C. Guo, X. Zhang, L. Wang, T. Hu, G. Mu, F. Huang, and X. Xie, npj Quantum Mater. **3**, 34 (2018).
[58]D. Prober, R. Schwall, and M. Beasley, Phys. Rev. B **21**, 2717 (1980).
[59]F. Gamble, F. DiSalvo, R. Klemm, and T. Geballe, Science **168**, 568 (1970).
[60]Y. Xing, P. Yang, J. Ge, J. Yan, J. Luo, H. Ji, Z. Yang, Y. Li, Z. Wang, Y. Liu *et al.*, Nano Lett. **21**, 7486 (2021).
[61]A. Ribak, R. M. Skiff, M. Mograbi, P. Rout, M. Fischer, J. Ruhman, K. Chashka, Y. Dagan, and A. Kanigel, Sci. Adv. **6**, eaax9480 (2020).
[62]A. Achari, J. Bekaert, V. Sreepal, A. Orekhov, P. Kumaravadivel, M. Kim, N. Gauquelin, P. Balakrishna Pillai, J. Verbeeck, F. M. Peeters *et al.*, Nano Lett. **22**, 6268 (2022).
[63]Y. Tanaka, H. Matsuoka, M. Nakano, Y. Wang, S. Sasakura, K. Kobayashi, and Y. Iwasa, Nano Lett. **20**, 1725 (2020).
[64]T. Samuely, D. Wickramaratne, M. Gmitra, T. Jaouen, O. Šofranko, D. Volavka, M. Kuzmiak, J. Haniš, P. Szabó, C. Monney, G. Kremer, P. L. Fèvre, F. Bertran, T. Cren, S. Sasaki, L. Cario, M. Calandra, I. I. Mazin, and P. Samuely, arXiv:2304.03074 (2023).
[65]N. Ng and T. M. McQueen, APL Mater. **10**, 100901 (2022).
[66]R. A. Klemm, Physica C **514**, 86 (2015).
[67]B. E. Brown and D. J. Beerntsen, Acta Crystallogr. **18**, 31 (1965).